Soft Matter

PAPER

View Article Online
View Journal

Cite this: DOI: 10.1039/c9sm00476a

The capillary interaction between pairs of granular rafts†

Antoine Lagarde, [a] Christophe Josserand [b] and Suzie Protière*[a]

When an object is placed at the surface of a liquid, its weight deforms the interface. For two identical spherical objects, such a deformation creates an attractive force, leading to the aggregation of the two-body system. Here, we experimentally investigate the interaction between two granular rafts, formed by the aggregation of dense millimeter-sized beads placed at an oil–water interface. The interfacial deformation created by such a two-dimensional object exceeds by at least an order of magnitude the deformation of a single bead. This leads to unusually high capillary forces which strongly depend on the number of particles. Likewise, because the raft grows in size as more particles are added, the viscous drag experienced increases along with the capillary attraction, leading to a non-trivial dependence of the balance of forces on the number of beads. By studying the relative motion of two granular rafts in relation with the interfacial deformation they generate, we derive a model for the observed speed profiles. With this work, we generalize how the capillary interaction between two non-identical complex structures evolves with their respective geometry.

Received 6th March 2019,
Accepted 24th June 2019

DOI: 10.1039/c9sm00476a

rsc.li/soft-matter-journal

1 Introduction

When a few identical objects are deposited on a fluid interface, a daily yet striking phenomenon occurs, during which the passive objects will spontaneously move towards one another. The implications of what could appear as a trivial experiment are countless. In Nature, fire ants use it to survive floods by aggregating into a floating raft,[1] while some animals are able to propel by deforming the water surface in a specific way.[2] This phenomenon is also used in industrial processes for the fabrication of macroscopic objects with a specific microstructure.[3–5]

The self-assembly of objects at a liquid interface relies on the interaction due to the surface deformation around each particle.[6] When the menisci around several objects overlap, capillary attraction (or repulsion) arises. Colloidal particles generate lateral forces due to the undulation of the contact line around their surface,[7–10] either because of surface roughness and wettability, or due to a non-spherical shape. The interface around the particle is then conveniently seen as a capillary multipole. For anisotropic colloids, the interaction depends strongly on the individual shapes,[11] giving rise to oriented aggregation either through a precise manufacturing of the form of each particle,[12] or thanks to a curved interface acting as a force field.[13]

For larger objects, another contribution comes from the particles' weight which deforms the surrounding interface by pushing the liquid down, an effect that can be taken into account through a generalized Archimedes' principle.[14] Models for such interactions have been developed almost exclusively for two identical rigid bodies.[15,16] In 1949, Nicolson[15] proposed a model using a linear superposition approximation of the interface deformations to describe the force of interaction between two floating bubbles at a liquid interface. This far-field calculation leads to an analytical formulation of the capillary force between identical objects (bubbles, solid sphere,...).[16,17] Good experimental agreement has been reported for the relative motion of a small number of large identical spheres.[18,19] However, most of these models and experiments concern individual and identical particles and no detailed investigations have been made so far to characterize the interactions between clusters of particles.

In this paper, we focus on such large objects, where dense millimeter-sized beads act as monopoles. We study the interaction between two granular rafts,[20,21] each formed by the aggregation of dense spherical beads into a single axi-symmetric object. Such 2-D structures are flexible and exhibit high deformations of the interface due both to their weight and their geometrical extension. The overall meniscus created by these large objects generates a specific raft–raft interaction that needs to be characterized. We quantify the dependence of the drag and the capillary force experienced by a raft on both its size and the size of the other interacting raft. The present study questions whether two assemblies of particles forming dense objects can interact as single

[a] Sorbonne Université, Centre National de la Recherche Scientifique, UMR 7190, Institut Jean Le Rond ∂'Alembert, F-75005 Paris, France.
E-mail: protiere@ida.upmc.fr
[b] LadHyX, CNRS, Ecole Polytechnique, UMR 7646, 91128 Palaiseau, France

† Electronic supplementary information (ESI) available. See DOI: 10.1039/c9sm00476a

entities, and investigates the influence of the clusters dimensions on their interactions.

2 Kinematics of two interacting granular rafts

2.1 Experimental setup

In a typical experiment, a thick layer of oil (kinematic viscosity $\nu = 50 \times 10^{-6}$ m^2 s^{-1}, density $\rho_o = 960$ kg m^{-3}, oil–water surface tension $\gamma = 38$ mN m^{-1}) is carefully poured into a tank of dimensions $0.2 \times 0.2 \times 0.25$ m filled with pure water. A precise number of particles n_A are sprinkled from above. Beads are deposited far away from one another, from every direction around the raft. Due to the very strong gravitational interaction between such objects the beads automatically aggregate into a compact axisymmetric raft. When using the beads presented in Table 1, we never observe a loosely packed assembly such as the one described in ref. 22 and 23. The raft size can be controlled by adding beads progressively (meaning the raft is made of precisely n_A particles), as represented in Fig. 1.

The same procedure is reproduced elsewhere in the tank, with n_B particles. The motion of the two rafts thus formed (respectively identified by the letters A and B) is recorded either from above or from the side by a camera at 250 frames per second. The properties of the various beads used in the experiments are summarized in Table 1, along with the approximate maximum number of particles n_{max} the corresponding raft can reach before sinking.[21]

At the oil–water interface, the capillary length $\ell_c = \sqrt{\gamma/((\rho_w - \rho_o)g)}$ is greatly increased by buoyancy effects, so that $\ell_c \approx 10$ mm (with ρ_w the density of water, and g the gravitational acceleration). The maximal possible deformation is thus far more important than at an air–water interface. This leads to unusually high long-range capillary forces.

2.2 Speed measurement

For a given set of sizes (n_A, n_B), we record the dynamics from above to measure the speed of the rafts, and from the side when we want to access the deformation of the interface. A typical experiment can be visualized in Fig. 2 (see ESI† for the movies, taken from above and from the side), for two rafts with respectively $n_A = 30$ and $n_B = 50$. The two rafts move towards one another until they come into contact, at which point they will rearrange to form a bigger raft or sink. Here, we focus on the interaction of two rafts before they reach contact.

Table 1 Characteristics of the beads used in experiments

Type of particle	ρ_s (kg m^{-3})	R_{part} (mm)	n_{max}
Plastic	1420	2	16
Plastic	1420	2.5	7
Ceramic	3800	0.35	160
Ceramic	3800	0.45	60
Ceramic	4800	0.35	60
Ceramic	4800	0.45	25

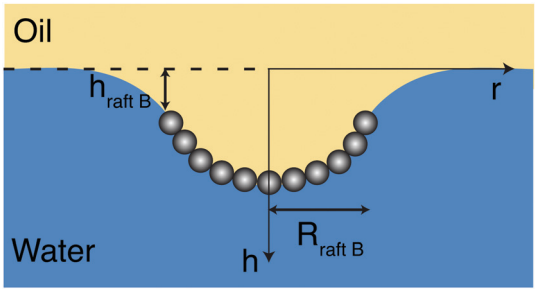

Fig. 1 Schematic side view of a granular raft. Deformation of the interface around a single raft B, described by two quantities: the radius of the raft $R_{raft\,B}$, and the depth of the interface at the edge of the raft $h_{raft\,B}$. The radial coordinates are defined from the center of the raft, while the origin of the vertical axis h corresponds to the height of the undisturbed flat interface.

In a typical experiment such as the one presented in Fig. 2a, the fluid interface undergoes strong deformations due to the weight of each raft. This induces a vertical displacement which cannot be neglected in our measurement of the raft speed. For example, in Fig. 2a, the amplitude of the vertical motion of raft B ($n_B = 30$) between the last two images is more than half the length of its horizontal motion. In our study, all the speed measurements are derived from top views of the granular raft motion. Yet, a movie taken from above only gives us information on the horizontal projection of the speed. The vertical component is not directly accessible. We deduce the vertical displacement from the radial motion, *via* measurements of the interface deformation.

The equation for the interface is obtained by a classic equilibrium between the hydrostatic pressure and the pressure jump due to the curvature. For a cylindrical coordinate system centered in the middle of the raft, the height of the interface beyond the raft B is obtained as the solution of the following system of equations:

$$\begin{cases} \gamma\left(\dfrac{h''}{1+h'^2} + \dfrac{h'}{r}\right) - (\rho_w - \rho_o)gh\sqrt{1+h'^2} = 0 \\ h(r \to \infty) = 0 \\ h(r = R_{raft\,B}) = h_{raft\,B} \end{cases} \quad (1)$$

with h the height of the interface ($h = 0$ for a flat interface), r the radial coordinate, h' the derivative of h with respect to r, $R_{raft\,B}$ the radius of the raft and $h_{raft\,B}$ the height of the interface at the edge of the raft (see Fig. 1). We neglect the irregularities at the edge of the raft due to the presence of the particles, making the assumption that the shape of the interface around the raft is isotropic. We can thus write eqn (1) in an axisymmetric configuration.

After having measured $R_{raft\,B}$ and $h_{raft\,B}$ from a side view of raft B (without the presence of A), we solve eqn (1) numerically, and obtain the expression of $h(r)$ imposed by the presence of the raft B. Then, from the knowledge of the radial position L of the center of A with respect to the center of B, which is measured directly from the movie, we can deduce the expected vertical position of the granular raft A along its motion.

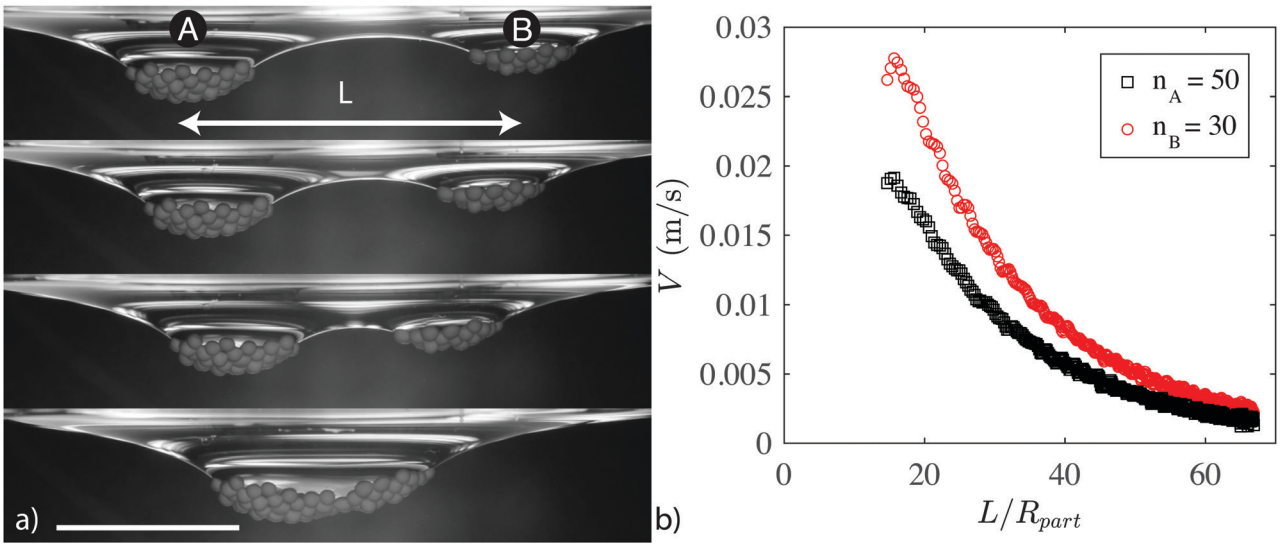

Fig. 2 Aggregation of two granular rafts. (a) Time lapse of the motion of two granular rafts at an oil–water interface, filmed from the side (see ESI† for the movies, taken from above and from the side). Each raft is made of ceramic spherical beads (density ρ_s = 3800 kg m^{-3}, radius of a single particle R_{part} = 0.45 mm), in an axisymmetric configuration, with 50 particles for the raft on the left (raft A), and 30 particles for the one on the right (raft B). The final image corresponds to the exact moment of contact between the two rafts. Time between two images: 0.13 s. Scale bar: 10 mm. (b) Speed of the same two rafts as a function of the distance between the centers of the two rafts (made dimensionless using the radius of a bead R_{part}). Red circles: speed of raft B; black squares: speed of raft A. The errors bars are of the order of the thickness of the curves.

Following this procedure, we can calculate the total speed V of a granular raft from its radial displacement. Implicitly here, we use the Nicolson linear approximation[15] by saying that the derivative of the vertical position of A only depends on the interface height imposed by B.

The total speed V for the experiment of Fig. 2a is plotted in Fig. 2b, for the two rafts, as a function of the non-dimensionalized distance between the two centers. As a consequence, the curves have to be read from right to left, with an increase of V as the two rafts get closer, until it reaches a maximum speed. Then, the two rafts briefly slow down just before contact, because of a hydrodynamic coupling in the drag force: the liquid that separates the two rafts before collision has to be expelled, causing an increase in the drag.

Qualitatively, we can already see in Fig. 2 that the sizes of the two rafts have an effect on their motion. Indeed a raft made of 30 particles will move at a larger speed than the raft made of 50 particles during their interaction. We now need a model to relate these speed profiles to the interacting forces acting on a granular raft.

3 Dynamics of two interacting granular rafts

3.1 Theoretical model

We study the influence of the number of particles on the respective motion of two granular rafts. To that end, we use the theoretical framework derived for the dynamics of two identical spheres interacting at an interface, in the limit of small deformations,[16] and see how the amplitude of the forces is affected by the size of the raft.

The force between two objects at an interface depends only on the shape of the interface around them, and is obtained by integrating the capillary forces around their contact line. This shape results from how the particles deform the interface, which in the case presented here is the consequence of the combined effect of their weight, their wettability and the induced buoyancy. In the case of small spheres ($R_{part} \ll \ell_c$) where the shape of the interface is isotropic around each bead and its deformations are small, the calculation leads to an energy of interaction equal to the product between the effective weight of one particle and the vertical deformation created by the other. For two identical spheres, the force exerted by one bead on the other is then obtained by deriving the interaction energy, leading to:

$$F_{cap\ 1\to1} = a(R_{part}, \rho_s, \ldots) K_1\left(\frac{L}{\ell_c}\right) \quad (2)$$

with a a coefficient taking into account the particle and fluid properties (ref. 16 for more details), L the distance between the centers of the two particles, and K_1 the modified Bessel function of the second kind of order one. We generalize this formulation to the attraction of two granular rafts (designated by the letters A and B), as schematically represented in Fig. 3:

$$F_{cap\ A\to B} = f(n_A, n_B) a(R_{part}, \rho_s, \ldots) K_1\left(\frac{L}{\ell_c}\right) \quad (3)$$

where f is the function we want to determine experimentally, $F_{cap\ A\to B}$ the force exerted by the raft A on B, and n_A and n_B the number of particles in each raft. To make such a generalization, we assume here that the wavelength and amplitude of the undulation of the edge of the raft are small enough so that they can be neglected at long range and the interface around

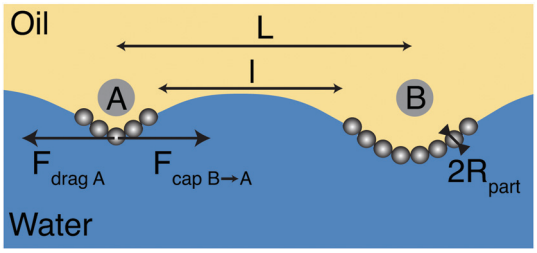

Fig. 3 Forces acting on a given axisymmetric granular raft. Schematic representation of the interaction between two granular rafts A and B (n_A and n_B respectively stand for the number of particles in each raft), at an oil–water interface. L is the distance between the centers of the two rafts, while l is the distance between the two nearest particles of each raft. The raft A (respectively B) is subjected to a capillary attraction $F_{\mathrm{cap\,B\to A}}$ and a viscous drag $F_{\mathrm{drag\,A}}$ (respectively $F_{\mathrm{cap\,A\to B}}$ and $F_{\mathrm{drag\,B}}$).

the raft can be described as isotropic. We neglect here the granular nature of the raft, the edge of which may be roughened by individual particles.

The drag force acting on a raft also needs a careful treatment. For two identical spherical beads, F_{drag} is expressed as a Stokes drag corrected by the mobility function G for two spheres in a single phase, in order to take into account the drainage of the liquid between the particles:

$$F_{\mathrm{drag}} = bVG^{-1}\left(\frac{L}{R_{\mathrm{part}}}\right) \qquad (4)$$

with V the speed of the particle, $b = 6\pi\mu_o R_{\mathrm{part}}k$ a corrected Stokes drag coefficient on a sphere, where k accounts for the fact that the particle moves along an interface and as a consequence is immersed in two phases.[24] The mobility function G was tabulated by Batchelor,[25] and can be approximated by an interpolation formula.[18] At infinity, there is no coupling and $G(+\infty) = 1$, whereas when the two particles are in contact, $G(2) = 0$.

Again, we generalize eqn (4) to the motion of a granular raft:

$$F_{\mathrm{drag\,A}} = g(n_A)bV_A G^{-1}\left(\frac{l+2R_{\mathrm{part}}}{R_{\mathrm{part}}}\right) \qquad (5)$$

where g is the function we want to determine experimentally, and l designates the distance between the edges of the two closest particles of the two rafts, as defined in Fig. 3. We approximate the hydrodynamic coupling between the two rafts by considering the drainage of the liquid only between the two closest particles of each interacting raft. Such a formulation of the drag is only valid for a sphere, but here we use it for a granular raft, which has the shape of a curved disk. As a consequence, the scaling law for the drag should also differ from the Stokes drag of a sphere: if the linearity with the viscosity and the velocity is expected from this viscous regime, the length involved cannot be a priori the radius of the raft.

Keeping in mind the assumption lying under the scaling law of eqn (5), we combine it with eqn (3) and finally deduce an expression for the speed of a raft made of n_A particles attracted by a second raft constituted by n_B beads:

$$V_A = \frac{f(n_A,n_B)}{g(n_A)}\frac{a}{b}G\left(\frac{l+2R_{\mathrm{part}}}{R_{\mathrm{part}}}\right)K_1\left(\frac{L}{\ell_c}\right) \qquad (6)$$

The ratio a/b is measured once and for all for each type of particle (given radius and given density, see Table 1) thanks to a two-bead experiment, for which $f(1,1) = g(1) = 1$ by definition. Then, f/g can be experimentally determined as a function of n_A and n_B, giving us information on the ratio of the two forces.

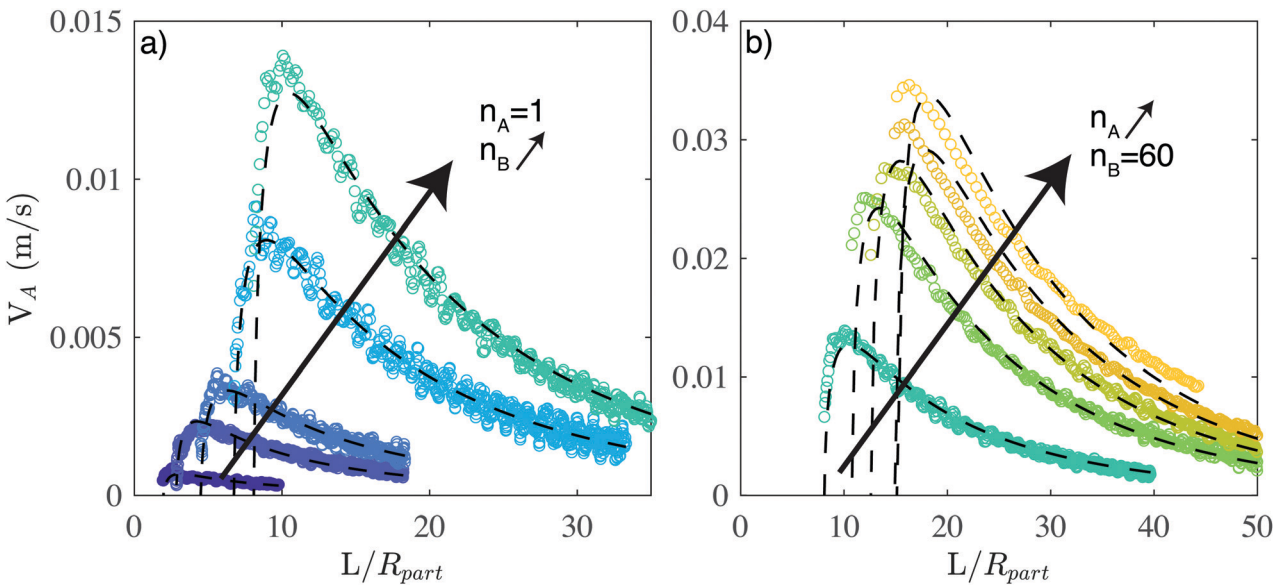

Fig. 4 Agreement between experimental results and theoretical model. Speed of the raft A for different number of particles in A and B, as a function of the distance between the centers of the two rafts (made dimensionless using the radius of a bead R_{part}), fitted by the theoretical prediction of eqn (6) (black dotted curves). For all these experiments, the particles are ceramic spherical beads (density ρ_s = 3800 kg m^{-3}, radius of a single particle R_{part} = 0.45 mm). (a) Speed of a single particle A for different sizes of the other raft, n_B = 1, 5, 10, 30, 60. (b) Speed of a raft of increasing size (n_A = 1, 5, 10, 20, 40), attracted by a raft of fixed size (n_B = 60). The errors bars are of the order of the thickness of the curves.

3.2 Experimental results

We plot in Fig. 4 the speed of the raft A as a function of the distance between the centers of the two rafts L, first with $n_A = 1$ and an increasing n_B, and then with $n_B = 60$ and an increasing n_A. The speed of the raft appears to increase both with n_A and n_B, as expected from our definition of the capillary force. This is due to the deformation of the interface that increases with n_B. Similarly, $F_{\mathrm{cap\,B\to A}}$ is related to the weight and the size of the raft A, an increasing quantity with n_A. Focusing on a single curve of Fig. 4, we recover the behavior described previously: an increasing speed as the two rafts are attracted towards one another, until a maximum where the speed then starts to decrease due to the drainage of the liquid between the two rafts. As n_A or n_B increases, the curves are shifted to the right since $L_{\min} = R_{\mathrm{raft\,A}} + R_{\mathrm{raft\,B}}$, a value which increases as we add particles.

The black dotted curves of Fig. 4 represent the fit of eqn (6) for each couple of rafts (n_A, n_B). There is a good agreement between the experimental data and the theory for $n_A = 1$ (Fig. 4a), the fitting line being within the experimental noise. As we increase n_A, the fit starts to drift from the measured speed, in particular regarding the position of its maximum. We discuss the limitations of our description in the last section of the paper and propose a number of hypothesis which may explain this result. Keeping in mind that for high n_A, our model does not explain the entire dynamics, we observe the evolution of the fitting coefficient f/g as a function of n_A and n_B for different types of beads (see Table 1), and a large variety of combinations of n_A and n_B (Fig. 5). All the data collapse onto the same straight line when represented as a function of $n_B\sqrt{n_A}$, on approximately three decades, giving the following experimental result:

$$\frac{f(n_A, n_B)}{g(n_A)} = n_B\sqrt{n_A} \tag{7}$$

Eqn (7) gives us an empirical relation between the ratio of the two forces and the number of particles in each raft. Even though both forces are functions of n_A, n_B only intervenes in the capillary force. This immediately proves that $F_{\mathrm{cap\,A\to B}} \propto n_B$. Moreover, applying Newton's third law,[26–28] we obtain that this force has to be symmetrical in n_A and n_B and thus $F_{\mathrm{cap\,A\to B}} \propto n_A n_B$, implying also for the drag force $g(n_A) \propto \sqrt{n_A}$. The far-field behavior of the capillary force $F_{\mathrm{cap\,A\to B}} \propto n_A n_B$ follows a Coulomb or gravitational-like law, replacing the electric charge or the mass by the number of grains; since this force only depends on the number of grains, it indicates that the organization of the particles within such compact granular rafts plays no role in the interaction. This is consistent with the superposition approximation, where interface deformation at large distances can be considered as the sum of the individual meniscii of each particle. However we lack a physical understanding of these scalings and need to go back to the definition of the capillary force.

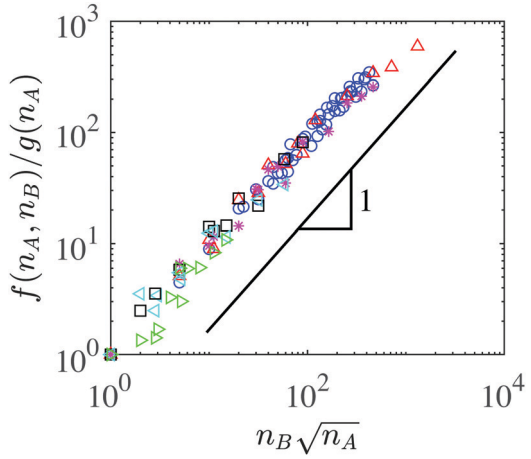

Fig. 5 Forces acting on a granular raft. Fitting coefficient of the speed of the granular raft A, as a function of $n_B\sqrt{n_A}$, for different densities and sizes of particles (green right-pointing triangles: plastic beads, ρ_s = 1420 kg m^{-3}, R_{part} = 2.5 mm; blue left-pointing triangles: plastic beads, ρ_s = 1420 kg m^{-3}, R_{part} = 2 mm; black squares: ceramic beads, ρ_s = 4800 kg m^{-3}, R_{part} = 0.45 mm; pink stars: ceramic beads, ρ_s = 4800 kg m^{-3}, R_{part} = 0.35 mm; blue circles: ceramic beads, ρ_s = 3800 kg m^{-3}, R_{part} = 0.45 mm; red upward-pointing triangles: ceramic beads, ρ_s = 3800 kg m^{-3}, R_{part} = 0.35 mm). The solid line has a slope of 1.

4 The drag and the capillary force

As explained earlier, the capillary force exerted by a raft, assuming it has an isotropic shape and the deformations of the interface are small, is proportional to the slope of the interface deformed by its presence. In the limit of small deformations we derive an analytical formula for this slope by solving a linearized version of eqn (1):

$$\begin{cases} \nabla^2 h = \dfrac{h}{\ell_c^2} \\ h(r \to \infty) = 0 \\ h(r = R_{\mathrm{raft}}) = h_{\mathrm{raft}} \end{cases} \tag{8}$$

which gives us the following expression:

$$\frac{\mathrm{d}h}{\mathrm{d}L} = \frac{h_{\mathrm{raft}}/\ell_c}{K_0(R_{\mathrm{raft}}/\ell_c)} K_1\left(\frac{L}{\ell_c}\right). \tag{9}$$

with K_0 the modified Bessel function of the second kind of order zero.

Eqn (9) can be reconciled with the scaling $F_{\mathrm{cap\,A\to B}} \propto n_A$ if we show that the modified aspect ratio of a raft $\dfrac{h_{\mathrm{raft}}/\ell_c}{K_0(R_{\mathrm{raft}}/\ell_c)}$ is linear with its number of particles n.

4.1 Experimental and numerical description of a raft shape

Experimentally, we measure h_{raft} from side views of the granular raft (blue arrows, Fig. 6a). We then measure the area of the raft A_{raft} from top views (see Video S2 of the ESI†) and calculate the equivalent radius by $R_{\mathrm{raft}} = \sqrt{A_{\mathrm{raft}}/\pi}$. The experimental modified aspect ratio is plotted in black diamonds in Fig. 6b for different types of beads and raft sizes, as a function of the effective weight

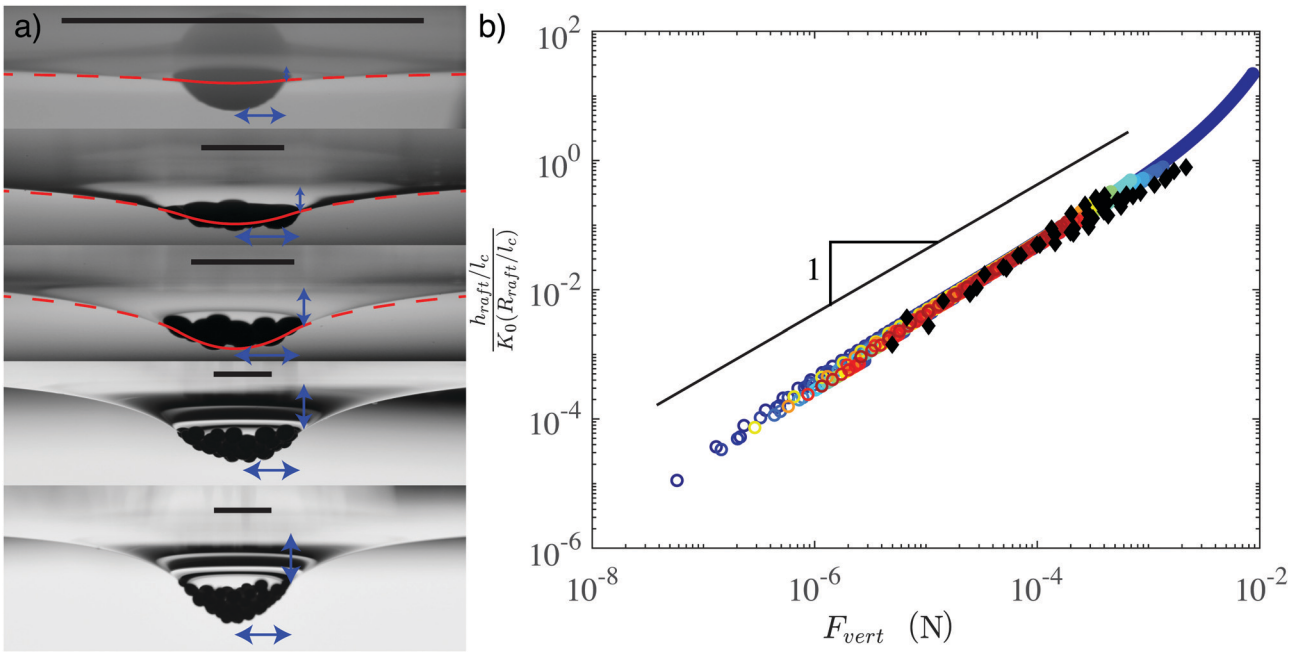

Fig. 6 Morphology and weight of a granular raft. Relation between the deformation of the interface and the weight of the granular raft, for a broad variety of densities, radii and numbers of particles. (a) Side view of a granular raft for an increasing number of ceramic particles (density ρ_s = 4800 kg m^{-3}, radius of a single particle R_{part} = 0.35 mm). In the top three photos, the red line represents the shape of the interface calculated by the numerical simulation for a membrane of a radius similar to the background photo (dotted line: oil–water interface, solid line: granular raft). The blue arrows indicate the measurement of R_{raft} and h_{raft}. Scale bars: 3 mm in each photo. (b) Modified aspect ratio $\frac{h_{raft}/\ell_c}{K_0(R_{raft}/\ell_c)}$ as a function of the effective weight of the raft F_{vert}, for experiments (black diamonds), and numerical simulations (colored circles). The solid line has a slope of 1. The vertical errors bars for the experiments are of the order of the size of the individual points, and are thus not displayed for clarity reasons.

of a raft F_{vert}, that we define as the difference between the weight of the particles and their buoyancy:

$$F_{vert}(n) = nF_{vert}(1) = n\frac{4}{3}\pi {R_{part}}^3 g\left(\rho_s - \frac{\rho_o + \rho_w}{2}\right) \qquad (10)$$

with n the number of particles in the raft. In eqn (10), both the weight and the buoyancy of the particles are considered linear with n, with the supplementary assumption that a bead is equally immersed in oil and water. However, we are aware that the generalized buoyancy of the raft, which takes into account surface tension effect, is not strictly additive, as discussed in previous collective sinking experiments.[14]

All the data collapse onto a single curve, and the modified aspect ratio appears linear with F_{vert} (a power law regression on the experimental data gives an exponent of 1.01), which is by definition proportional to n. As a consequence, the modified aspect ratio is linear with the number of particles.

To this experimental evidence, we add a numerical confirmation for the morphology of a granular raft, using the code described in ref. 21. The raft is simulated as an axisymmetric continuous membrane of thickness $2R_{part}$, with a given volume fraction of a material of density ρ_s, a complementary volume fraction of a material of density $(\rho_o + \rho_w)/2$, and a tension $\vec{T}$ directed tangentially to the raft surface. As long as the tension remains positive, a static solution is found, and the shape of both the granular raft and the interface beyond can be solved numerically.

In Fig. 6a, the simulated interface is plotted on top of experimental visualisations of the corresponding granular raft, with a visually good agreement for the top three photos. For the last two granular rafts shown in Fig. 6a, no numerical result is available: the simulations predict the sinking of the raft for such a deformation. This is probably due to the simplicity of the model used for the simulations, the limitations of which are discussed in our previous work.[21] As a consequence, the numerics can only give us information for part of the sizes accessible experimentally. However, they allow us to explore a far broader range of densities and radii of particles, and appear in that sense complementary to the experiments. The numerical measurement of the modified aspect ratio is represented in colored circles in Fig. 6. Here again, the data collapse onto the same curve when represented as a function of F_{vert}, over more than four decades, with an exponent of 1.08 for a power fitting law. In conclusion, we recover the following result both experimentally and numerically:

$$\frac{h_{raft}/\ell_c}{K_0(R_{raft}/\ell_c)} \propto n \qquad (11)$$

Interestingly, in Fig. 6b, we find that beyond a critical vertical force, the linear relation between the modified aspect ratio and F_{vert} no longer holds (see the right portion of the blue curve). Such a curve corresponds to a situation where the raft reaches a maximal depth which corresponds to a balance

between the hydrostatic pressure and the raft weight, and then extends indefinitely as more particles are added.[21] As a consequence, h_{raft} is bounded, leading to the saturation of the capillary force. Since $K_0(R_{\mathrm{raft}}/\ell_c) \sim \sqrt{\frac{\pi}{2R_{\mathrm{raft}}}}\,e^{-R_{\mathrm{raft}}}$ and $F_{\mathrm{vert}} \propto {R_{\mathrm{raft}}}^2$, it explains the vertical deviation in Fig. 6b for large rafts.

Eqn (11) can also be recovered theoretically in the limit of small deformations (see ESI† for more details). All these results validate that:

$$F_{\mathrm{cap\,B\to A}} = n_A n_B F_{\mathrm{cap\,1\to 1}}. \quad (12)$$

4.2 The drag force on each raft

Finally, we need to explain how the drag force depends on the raft geometry:

$$F_{\mathrm{drag\,A}} = \sqrt{n_A} F_{\mathrm{drag\,1}} \quad (13)$$

One could understand the drag dependency with n_A by considering the equivalent sphere of radius R_{raft}. For such a sphere, the Stokes drag is proportional to R_{raft}, which for a large range of granular raft sizes evolves as $\sqrt{n}$. This argument does not hold for the largest granular rafts (see for instance the last photo of Fig. 6), for which the high curvature of the raft makes R_{raft} deviate from this law. However at first order, $R_{\mathrm{raft}} \propto \sqrt{n}$, leading to the expected drag on the granular raft. The proportionality between the drag force and the raft radius is still quite surprising, since the shape of a granular raft is not a perfect sphere, but more a curved disk.

5 Discussion

A number of hypotheses underlying the approach described in this paper are no longer valid for a granular raft. They give us some clues to understand the limits of our model. In particular we observe an increasing discrepancy between the fit and the experimental data measured for the velocities when the rafts become large (the two highest velocities of Fig. 4b for n_A = 20 and 40). The two-sphere canonic example we use to derive eqn (3) and (5) strongly relies on the assumption of small deformations around spherical beads (small in relation to the capillary length). With granular rafts, we can reach a vertical deformation of the interface up to almost half the capillary length. Moreover, the morphology of a raft, a two-dimensional circular monolayer of beads, cannot be approximated as a spherical shape, and one could therefore expect the drag to be drastically different. Finally, the viscous hypothesis used for the calculation of the drag can be questioned for the bigger rafts. In this case, the maximum speed reached during their motion is almost a hundred times higher than for two single beads, leading to a Reynolds number of order one. All these differences may change the amplitude of the forces through f and g and even the form of these functions.

We also assumed that the capillary force is proportional to $K_1(L/\ell_c)$, a result that comes from the linearized solution of eqn (1). However, for some experiments, when two dense granular rafts interact, as in Fig. 7, eqn (1) becomes highly non-linear, and the approximate linear solution is no longer sufficient to account for the curvature of the interface. Fig. 7 illustrates this limitation of our model: on top of the experimental visualisation of the interface when two granular rafts are almost in contact, we plot the interfacial shape we would get if the deformations could be superimposed, deduced from the experimental measurement of the shape of the interface around a single granular raft of the same size. The superposition principle seems to account rather well for the curvature on the left and right side of each raft, but clearly overestimates the depth of the interface between the two rafts, leading to an error on the calculation of the capillary force. This could be part of the explanation for the disagreement between the fit and the measured speed in Fig. 4 for the motion of the two biggest rafts.

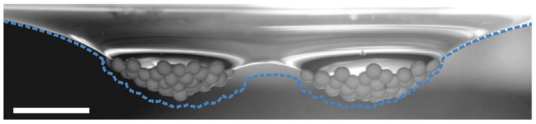

Fig. 7 Example of the failure of the linear superposition assumption. Comparison between a side view of two granular rafts during their motion towards one another (background photo) and the expected interfacial shape obtained if the assumption of small deformations was valid (blue dotted curve). Each of the rafts is made of 50 ceramic spherical beads (density ρ_s = 3800 kg m^{-3}, radius of a single particle R_{part} = 0.45 mm), in an axisymmetric configuration. The photo is taken 0.1 s before contact. Scale bar: 5 mm.

Another important feature that we did not take into account is the lateral extension of a granular raft. As already emphasized, the derivation of eqn (2) for the capillary force between two spheres at an interface relies on various hypotheses, including the size of the particles: $R_{\mathrm{part}} \ll \ell_c$. However, the largest rafts, as illustrated in Fig. 7 for instance, can exhibit a diameter of the order of the capillary length. In this situation eqn (2) should not be valid anymore. Here again, this could explain the discrepancy between our experimental data and the corresponding fitting curve for large rafts.

Despite all these limits, our model still accounts for the major part of our data, proving that in a first approximation, a granular raft does behave as a heavy membrane which is not deformed by the interaction with other rafts.

6 Conclusion

We have investigated the interaction dynamics of a two-body system formed after the clustering of beads into granular rafts at an oil–water interface. In particular we described the capillary forces generated by each granular raft, as well as the drag due to their individual motion. Because the deformation around a granular raft strongly depends on its size (depth and width), the capillary interaction can surpass by several orders of magnitude the forces created by individual beads, with a very strong dependence on the number of particles. A generalization of

the two-particle model is found to account very satisfactorily for the motion of the granular rafts, and only starts to deviate from the experimental data for objects of dimensions close to the capillary length. Despite the clear non-linearity of the equations describing the shape of the interface for such large rafts, the capillary force appears linear both with the size of the attracting and the attracted raft. The drag, on the other hand, increases linearly with the radius of the considered raft (or in other terms, as the square root of the number of particles).

In this paper we have completely neglected the intrinsic discrete nature of a granular raft by modeling it as a two-dimensional membrane. However, in some cases the granular aspect of the raft may play an important role. We have observed that rafts made of smaller particles (diameter <400 μm) show a weaker cohesion between the grains within the raft, which may lead to erosion and internal motions for a fast enough raft displacement. Further work is thus required to characterize this phenomenon and investigate the role of shape changes on the overall interaction of granular objects at a liquid interface. Discrete aspects of the raft, as well as elasticity, could be also included in future developments of the model.

Conflicts of interest

There are no conflicts to declare.

Notes and references

1 N. J. Mlot, C. A. Tovey and D. L. Hu, *Proc. Natl. Acad. Sci. U. S. A.*, 2011, **108**, 7669–7673.
2 D. L. Hu and J. W. Bush, *Nature*, 2005, **437**, 733.
3 U. Srinivasan, D. Liepmann and R. T. Howe, *J. Microelectromech. Syst.*, 2001, **10**, 17–24.
4 T. D. Clark, J. Tien, D. C. Duffy, K. E. Paul and G. M. Whitesides, *J. Am. Chem. Soc.*, 2001, **123**, 7677–7682.
5 N. Bowden, A. Terfort, J. Carbeck and G. M. Whitesides, *Science*, 1997, **276**, 233–235.
6 P. A. Kralchevsky and K. Nagayama, *Adv. Colloid Interface Sci.*, 2000, **85**, 145–192.
7 K. D. Danov, P. A. Kralchevsky, B. N. Naydenov and G. Brenn, *J. Colloid Interface Sci.*, 2005, **287**, 121–134.
8 K. D. Danov and P. A. Kralchevsky, *Adv. Colloid Interface Sci.*, 2010, **154**, 91–103.
9 L. Botto, E. P. Lewandowski, M. Cavallaro and K. J. Stebe, *Soft Matter*, 2012, **8**, 9957–9971.
10 D. Stamou, C. Duschl and D. Johannsmann, *Phys. Rev. E: Stat. Phys., Plasmas, Fluids, Relat. Interdiscip. Top.*, 2000, **62**, 5263.
11 I. B. Liu, N. Sharifi-Mood and K. J. Stebe, *Annu. Rev. Condens. Matter Phys.*, 2018, **9**, 283–305.
12 E. P. Lewandowski, J. A. Bernate, A. Tseng, P. C. Searson and K. J. Stebe, *Soft Matter*, 2009, **5**, 886–890.
13 M. Cavallaro, L. Botto, E. P. Lewandowski, M. Wang and K. J. Stebe, *Proc. Natl. Acad. Sci. U. S. A.*, 2011, **108**, 20923–20928.
14 D. Vella, *Annu. Rev. Fluid Mech.*, 2015, **47**, 115–135.
15 M. Nicolson, *Mathematical Proceedings of the Cambridge Philosophical Society*, 1949, pp. 288–295.
16 D. Vella and L. Mahadevan, *Am. J. Phys.*, 2005, **73**, 817–825.
17 W. Gifford and L. Scriven, *Chem. Eng. Sci.*, 1971, **26**, 287–297.
18 N. D. Vassileva, D. van den Ende, F. Mugele and J. Mellema, *Langmuir*, 2005, **21**, 11190–11200.
19 M.-J. Dalbe, D. Cosic, M. Berhanu and A. Kudrolli, *Phys. Rev. E: Stat., Nonlinear, Soft Matter Phys.*, 2011, **83**, 051403.
20 M. Abkarian, S. Protière, J. M. Aristoff and H. A. Stone, *Nat. Commun.*, 2013, **4**, 1895.
21 S. Protière, C. Josserand, J. M. Aristoff, H. A. Stone and M. Abkarian, *Phys. Rev. Lett.*, 2017, **118**, 108001.
22 N. Xue, S. Wu, S. Sun, D. Quéré and Q. Zheng, *Langmuir*, 2014, **30**, 14712–14716.
23 J.-C. Loudet, A. M. Alsayed, J. Zhang and A. G. Yodh, *Phys. Rev. Lett.*, 2005, **94**, 018301.
24 A. Dani, G. Keiser, M. Yeganeh and C. Maldarelli, *Langmuir*, 2015, **31**, 13290–13302.
25 G. Batchelor, *J. Fluid Mech.*, 1976, **74**, 1–29.
26 P. A. Kralchevsky and K. Nagayama, *Langmuir*, 1994, **10**, 23–36.
27 V. Paunov, P. Kralchevsky, N. Denkov, I. Ivanov and K. Nagayama, *Colloids Surf.*, 1992, **67**, 119–138.
28 O. D. Velev, N. D. Denkov, V. N. Paunov, P. A. Kralchevsky and K. Nagayama, *Langmuir*, 1993, **9**, 3702–3709.

